Journal Pre-proof

Blue-light excitable $La_2Ce_2O_7:Eu^{3+}$ red phosphors for white light-emitting diodes

Shikao Shi, Lina Wang, Ming Fang, Lianshe Fu, Luís D. Carlos, Rute A.S. Ferreira, Jiye Wang, Shuping Wang

PII: S0925-8388(19)33472-3

DOI: https://doi.org/10.1016/j.jallcom.2019.152226

Reference: JALCOM 152226

To appear in: *Journal of Alloys and Compounds*

Received Date: 3 July 2019

Revised Date: 5 September 2019

Accepted Date: 9 September 2019

Please cite this article as: S. Shi, L. Wang, M. Fang, L. Fu, Luí.D. Carlos, R.A.S. Ferreira, J. Wang, S. Wang, Blue-light excitable $La_2Ce_2O_7:Eu^{3+}$ red phosphors for white light-emitting diodes, *Journal of Alloys and Compounds* (2019), doi: https://doi.org/10.1016/j.jallcom.2019.152226.

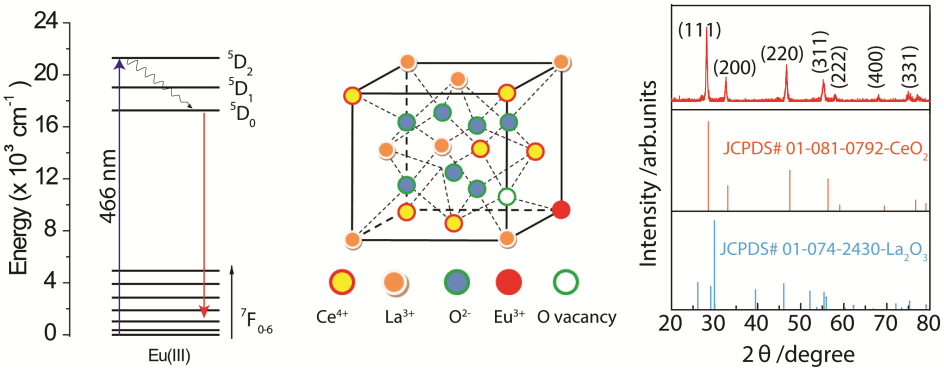

Blue-light excitable $La_2Ce_2O_7:Eu^{3+}$ red phosphors for white light-emitting diodes

Shikao Shi[a,*], Lina Wang[a], Ming Fang[b], Lianshe Fu[b], Luís D. Carlos [b,*], Rute A. S. Ferreira [b,*], Jiye Wang[a] and Shuping Wang[a]

[a]*College of Chemistry and Materials Science, Key Laboratory of Inorganic Nanomaterials of Hebei Province, Hebei Normal University, Shijiazhuang 050024, China.*

[b]*Physics Department and CICECO - Aveiro Institute of Materials, University of Aveiro, 3810-193 Aveiro, Portugal.*

* Corresponding authors: E-mail addresses, shishikao@hebtu.edu.cn (S. Shi), lcarlos@ua.pt (L.D. Carlos, rferreira@ua.pt (R.A.S. Ferreira).

Abstract

Inorganic phosphors which can be effectively excited with blue-light are highly desirable for white light-emitting diodes (WLEDs). Herein, Eu^{3+}-activated $La_2Ce_2O_7$ phosphors are prepared by a self-rising reaction using urea and glycine as leavening agents under hydrothermal conditions. The phosphors display a well-distributed round or elliptical particle shapes with an average diameter of about 55±10 nm. The excitation spectrum is dominated by the $^7F_0 \rightarrow {}^5D_2$ transition (~466 nm) that overlaps the emission of efficient blue LEDs, rendering these phosphors as very attractive as blue converters. The luminescence performance can be effectively improved by optimizing the molar ratios of leavening agents and the content of Eu^{3+} concentration and, thus, the absolute quantum yield can reach 0.229±0.023. By combining a commercial blue LED chip (InGaN, 465 nm) and the phosphors, intriguing efficient pure red emission is achieved with CIE color coordinates of (0.669,0.330). This pure red emission is used to tune the well-known poor correlated color temperature values of WLEDs based on YAG:Ce^{3+}. WLEDs are fabricated by coating blue LED chips with blends of YAG:Ce^{3+} and Eu^{3+}-activated $La_2Ce_2O_7$, yielding prototypes with enhanced color rendering index that is easily adjusted from 7119 to 3242 K, demonstrating that this strategy may use to complement the red component in WLEDs.

Keywords: Europium; red phosphor; photoluminescence; blue converter; white light-emitting diode

1. Introduction

The International Energy Agency estimated the total electrical energy consumptions for lighting loads of about 19% worldwide [1] (the number for USA is about 10% accordingly to the U.S. Energy Information Administration [2]). Energy consumption, with the depletion of fossil-based fuel reserves, has become problematic, creating several challenges, and gained increased attention worldwide. The cumulative global energy crisis is, then, demanding high energy-efficient lighting systems that can help to conserve energy and reduce lighting costs. Nowadays, great efforts have been devoted to the development of alternative lighting devices to replace traditional illumination lamps in order to save energy. In this regard, WLEDs have emerged as an important class of lighting devices that has been used to replace conventional lighting due to their admirable merits such as extraordinary efficiency, lower energy consumption, longer operation lifetime, environmental friendly characteristics, compactness and robustness and have been considered as the next-generation light source [3]. The high color saturation and reproducibility of WLEDs render these devices competitive in color perception.

Currently, commercial WLEDs are based on $Y_3Al_5O_{12}:Ce^{3+}$ ($YAG:Ce^{3+}$) broad-band yellow phosphor in combination with blue LED chips through a low cost and simple procedure, in which the yellow phosphor converter $YAG:Ce^{3+}$, dispersed in epoxy or silicone, is directly packed on the blue InGaN chip [4]. When driven by a certain current, the emitted yellow light from $YAG:Ce^{3+}$ pluses the transmitted blue light to constitute the white light. This type of WLEDs usually exhibits high luminous efficacy (LE, ~100 lm/W) [5]. However, in practical applications, such design suffers from some technical weaknesses. The two-color-based WLEDs exhibit the disadvantages of low color

rendering index (CRI, usually <75), high correlated color temperature (CCT, 4500–8000 K) and chromaticity drifts due to the intrinsic absence of efficient red light emission from YAG:Ce^{3+}, which only give cool white light and inevitably limit its applications in indoor or back lighting. In addition, the poor thermal stability and weak thermal conductivity of the organic binders result in gradual luminous attenuation and color-shift of the phosphors under long-term heat radiation [6,7].

In order to overcome these shortcomings, a red phosphor with excitation of blue light should be integrated into the package of WLEDs, which will then enable the realization of a warm white light with high CRI (>85) and low CCT (3000–4500 K) to meet the standard applications in indoor lighting [8]. This is an issue for most applications including home lighting where warm white light with a high CRI is required. As a result, it is desired to develop blue-light excited red phosphors with sharp emission peaks, high luminescence efficiency and sufficient chemical durability for mixing with the YAG:Ce^{3+} yellow phosphor to improve the performance of WLEDs.

During the last decades, extensive efforts have been devoted to developing novel red-emitting phosphors for WLED applications in order to improve the CRI and CCT parameters [9–15]. For this purpose, red phosphors should absorb strongly the blue emission (~460 nm) from InGaN chip and ideally have narrow emission bands centred at about 610 nm, which match the peak human eye sensitivity to red light [10]. For instance, Eu^{2+}- or Ce^{3+}-activated nitrides, $Sr_2Si_5N_8$:$Eu^{2+}$and $M_2Si_5N_8$:Ce^{3+} (M=Ca, Sr, Ba) [11,12], show high emission output, wide excitation band in the blue region, high chemical stability and small thermal quenching. However, these nitride phosphors still have some inherent disadvantages such as emission band extends to the deep red region (λ>640 nm),

serious re-absorption phenomenon and high production cost [16]. On the other hand, tetravalent manganese ions (Mn^{4+}) activated fluoride phosphors, $A_2MF_6:Mn^{4+}$ (A=alkali metal ion; M=Si, Ge, Zr, Sn, and Ti), bring sufficient blue absorption and match well with InGaN chip radiation [17]. Nevertheless, these Mn^{4+}-doped fluorides still have some disadvantages such as "non-green" synthesis conditions, susceptibility to degradation under high temperature and poor heavy moisture resistance [18].

Lanthanide (Ln) oxide phosphors show higher chemical stability with an eco-friendly preparation procedure. The Eu^{3+}-activated phosphors for blue LED chips usually exhibit weak emission due to either the low absorption in blue region from parity-forbidden 4*f*–4*f* transitions or mismatch excitation wavelength in the UV region from charge transfer band (CTB). For instance, Eu^{3+}-doped CeO_2 shows weak absorption in the blue region and can only be a potential candidate for UV-based LEDs [19]. Also, the LE of CeO_2:Eu is very low that limits its applications in solid-state lighting. It is, therefore, very desirable to find alternative red phosphors with high absorption in the blue region and strong red line-emission [20]. Recently, it was reported that the Eu^{3+}-doped $2CeO_2–0.5La_2O_3$ phosphors prepared by a solution combustion reaction showed enhanced luminescence when the Eu^{3+} ions occupied Ce^{4+} rather than La^{3+} sites, which was due to the concentration change of oxygen vacancy [21]. Furthermore, La-doped CeO_2 composite with 1:1 molar ratio of La:Ce, $La_2Ce_2O_7$, has been studied as a thermal barrier-coating material for high-temperature applications and proton conductor under reducing atmosphere [22,23]. Moreover, Eu^{3+}-doped $CeO_2–La_2O_3$ composites can overcome some of the above mentioned limitations of CeO_2:Eu materials and the luminescence properties of Eu-doped $La_2Ce_2O_7$ have been seldom reported [24]. In order to develop a green eco-friendly

preparation method for blue-light excitable Eu^{3+}-based red phosphors, the Eu^{3+}-doped CeO_2–La_2O_3 phosphors, $La_2Ce_{2-x}O_{7-x/2}$:xEu (x=0.1–0.9), were prepared in this work by a hydrothermal self-rising process assisted with mixed urea/glycine as leavening agent. The structural characterization, surface morphology and luminescence performance of the composites were performed and compared with those of CeO_2:Eu. Red emitting diodes were fabricated and their luminescence performances were characterized using commercial blue chips (465 nm) coated with the Eu^{3+}-activated $La_2Ce_2O_7$ phosphor. Moreover, as the pure red emission of this phosphor is obtained under analogous conditions found in commercial WLEDs combining a blue chip and the commercial YAG:Ce^{3+} yellow phosphor, we fabricate innovative WLEDs by coating the blue chips with blends formed by distinct proportions of YAG:Ce^{3+} and Eu^{3+}-activated $La_2Ce_2O_7$. The luminescence performance of the devices confirms that this strategy allows overcoming the low amount of red emission that limits the performance of the current used WLEDs.

2. Experimental section

2.1. Preparation of red phosphors

A series of Eu^{3+}-doped blue-light excitable red phosphors were prepared by self-rising method under hydrothermal condition. The starting materials include $Ce(NO_3)_3{\cdot}6H_2O$ (Yongda Chemical, Tianjin, A.R.), Eu_2O_3 (Institute of Non-ferrous Metals, Beijing, 99.99%), La_2O_3(Institute of Non-ferrous Metals, Beijing, 99.95%), urea (A.R.) and glycine (A.R.). All of them were used as received without further purification. In addition, $La(NO_3)_3$ and $Eu(NO_3)_3$ aqueous solutions were prepared by dissolving the related oxides with dilute nitric acid.

It was proved that the Eu^{3+}-doped $2CeO_2–0.5La_2O_3$ system showed enhanced luminescence when the Eu^{3+} ions are located in the Ce^{4+} site rather than in the La^{3+} one [21]. Therefore, in this study, $La_2Ce_{2–x}O_{7–x/2}$:xEu phosphors were synthesized with the Eu^{3+} ions located in the Ce^{4+} site. First, the Ln (La, Ce and Eu) nitrate solutions were mixed together in a molar ratio of 2, 2–x and x, for La, Ce and Eu, respectively. Then, the single urea or mixed urea/glycine (5-fold of the total Ln molar amount) as leavening agent was added to the mixed solution (about 50 mL) that was put into autoclave at 160 ^oC for 180 min to perform the self-rising reaction under hydrothermal conditions. During the self-rising reaction, the organic leavening agent was decomposed to NH_3 and CO_2, and the aqueous solution was gradually changed to emulsion. The emulsion was put into crucible and heated in a furnace at 500 ^oC for 30 min to move away the residual organic content. Finally, the samples were formed via heat-treatment at 950 ^oC for 2 h. When single urea was used, the sample seemed to be a mixture of CeO_2 and La_2O_3, implying that the compound was not appropriately formed. On the contrary, when the mixed urea/glycine was used, the as-prepared product was confirmed as a pure $La_2Ce_2O_7$ compound. For comparison, CeO_2:Eu was also prepared by similar way.

2.2. Fabrication of red-emitting LED and WLED prototypes

The $La_2Ce_{2–x}O_{7–x/2}$:xEu (x=0.7) particles were used to produce an LED device emitting in the red spectral region by coating a commercial blue LED chip emitting at 465 nm (RLS-B465, Roithner Laser technik, GmbH). The fine powder (250 mg) and polymethylmethacrylate (PMMA, 50 mg) were dissolved in 2 mL of $CHCl_3$ under stirring. The resulting mixture was further stirred at room temperature to get a homogenous solution. This solution was used to coat the commercial blue LED by dip-coating. This procedure was repeated until the LED surface was totally covered.

To fabricate WLEDs, the two-part, semi-rigid commercial polyurethane resin (UR5634polyurethane resin, Electrolube, UK) with 1:1 weight ratio were used to encapsulate the commercial yellow-emitting YAG:Ce^{3+} and the red-emitting $La_2Ce_{2-x}O_{7-x/2}$:xEu (x=0.7) phosphors. Before coating the blue-emitting LED chips (RLS-B465, Roithner Laser technik, GmbH), the polyurethane resin, YAG:Ce^{3+} and $La_2Ce_{2-x}O_{7-x/2}$:xEu (x=0.7) with 160:3:150 of weight ratio were completely blended. After coating, the LED prototypes were moved into an oven at 60 ^{o}C for 2 h for gelation.

2.3. Characterization

The crystal structure of the samples was checked by X-ray powder diffraction (XRD) using a D8 Advance X-ray powder diffractometer with CuKα (1.54056 Å) radiation. The scanning angle 2θ ranges from 20 to 80^{o}. The internal structure and oxygen vacancies were analyzed by a HORIBA JY HR800 confocal microscope Raman spectrometer and an Ar-ion laser (514.5 nm). The particle morphology and size were measured by an S-4800 field emission scanning electron microscope. The photoluminescence emission and excitation spectra were recorded by an F-4600 fluorescence spectrometer equipped with a 65 W Xenon lamp as the excitation source. The photoluminescence decay curves were acquired by an Edinburgh FS5-TCSPC spectrofluorometer. Additionally, the excitation and emission spectra of the optimal $La_2Ce_2O_7$:Eu and CeO_2:Eu samples were recorded using a Fluorolog3® Horiba Scientific (Model FL3-22) spectroscope. The excitation source was a 450 W Xe arc lamp. The emission spectra were corrected for detection and optical spectral response of the spectrofluorometer and the excitation spectra were corrected for the spectral distribution of the lamp intensity using a photodiode reference detector. The absolute emission quantum yields were measured using the Quantaurus-QY Plus C13534 (Hamamatsu) system with a 150 W xenon lamp coupled to a monochromator

for wavelength discrimination, an integrating sphere as the sample chamber, and a multichannel analyzer for signal detection. All the measurements were carried out at room temperature.

The LED emission spectra, the Commission International de l'Eclairage (CIE) color coordinates, the radiant flux (W), the luminous flux (lm), the CRI Ra and CCT values were measured using an integrating sphere ISP 150L-131 from Instrument Systems. The integrating sphere ($BaSO_4$ coating) has internal diameter of 150 mm and was coupled to an array spectrometer MAS 40 from Instrument Systems. The measurements are accurate within 5% according to the manufacturer specification.

3. Results and discussion

3.1. Structural Characterization

The XRD patterns of the undoped as-prepared powders are shown in Fig. 1a. For comparison purposes, the standard card data of CeO_2 (space group: Fm3m; JCPDS 01-081-0792) [25] and La_2O_3 (space group: P63/mmc; JCPDS 01-074-2430) [26] are also displayed in Fig. 1a. When only urea is used in the self-rising process, a mixture of CeO_2 and La_2O_3 is observed, even after the sintering process. When urea/glycine mixture is used, however, the XRD pattern corresponds to the previous reported $La_2Ce_2O_7$ structure [24], with the main diffraction peaks at 28.1, 32.6, 46.6, 55.2, 57.9, 67.9 and 75.0^o indexed to the (111), (200), (220), (311), (222), (400) and (331) crystallographic planes, respectively. The $La_2Ce_2O_7$ composite has a cubic fluorite structure, which is almost the same as CeO_2, except that of lattice parameter. Thus, the use of urea/glycine mixture is beneficial to the formation of the phase-pure phosphor. The reason for this is due to the addition of glycine, which acts not only as a leavening agent but also as a surfactant [27,28]. In addition, the amount of glycine also plays a

crucial role in determining the sample purity and crystallinity. The molar ratio of glycine to the total Ln amount has been optimized (0.7:1), which can be clearly confirmed in the XRD patterns (see Fig. S1). In the following parts, all the Eu^{3+}-doped $La_2Ce_2O_7$ samples were prepared at this molar ratio.

The XRD patterns of the $La_2Ce_{2-x}O_{7-x/2}$:xEu (x=0.0, 0.1, 0.3, 0.5, 0.7 and 0.9) phosphors are given in Fig. 1b. The XRD peaks of all Eu^{3+}-doped samples are similar to that of $La_2Ce_2O_7$, implying that the Eu^{3+} doping has little influence on the phosphor structure. In fact, the observed left-shift of the XRD peaks after Eu^{3+} doping is due to the ionic radius difference between Eu^{3+} ions (r = 1.21 Å) and Ce^{4+} ions (r =1.11 Å) [29], demonstrating that the Eu^{3+} ions have entered into the host lattice and located at the Ce^{4+} sites.

The microstructure and the surface morphology of the Eu^{3+}-doped $La_2Ce_2O_7$ phosphor, $La_2Ce_{1.3}O_{6.65}$:0.7Eu, were analyzed by SEM (Fig. 2a and 2b). The precursor powders (without any heat treatment) are not well crystallized (Fig. 2a), but after the self-rising and subsequent sintering process (950 ^oC for 2 h), the phosphors are crystalline (Fig. 2b), in agreement well with the appearance of distinct diffraction peaks in XRD patterns (Fig. 1a and 1b). Moreover, most of the particles display a well-distributed round or elliptical shapes, with an average diameter around 55±10 nm (Fig. 2c). The spherical particle shape, uniform size and low agglomeration degree are important factors to promote the application of phosphor powder for WLEDs [30].

FT-Raman spectra of $La_2Ce_{1.9}O_{6.95}$:0.1Eu (low doping concentration) and $La_2Ce_{1.3}O_{6.65}$:0.7Eu (high doping concentration) are measured to have further insight on the internal structure of the phosphors (Fig. 3). The strong Raman band between 390 and 495 cm^{-1} results from the oxygen breathing vibrations around the Ce^{4+} ions [31], whereas the weak peak between 495 to 670 cm^{-1} is due to the existence of oxygen vacancies [32,33]. While the maximum of the former band (at

about 450 cm^{-1}) does not change with the Eu^{3+} concentration, the weak peak is shifted from 565 to 583 cm^{-1} as the Eu^{3+} doping concentration increases from 0.1 to 0.7. This quite large shift indicates that the amount of oxygen vacancies is closely related to the Eu^{3+} concentration. Moreover, with the increase of Eu^{3+} doping concentration, the intensity of the strong peak at around 450 cm^{-1} dramatically decreases and in the meanwhile, the weak peak at around 583 cm^{-1} that ascribed to oxygen vacancies further increases, implying that the introduction of Eu^{3+} activators increases the oxygen vacancies amount in the lattice.

3.2. Optical Characterization

The excitation and emission spectra of $La_2Ce_{2-x}O_{7-x/2}$:xEu (x=0.1–0.9) composites are shown in Figs. 4a and 4b, respectively. The excitation spectra were monitored within the $^5D_0 \rightarrow {}^7F_2$ transition. The spectra are almost independent of the Eu^{3+} concentration being formed of a very low-intensity CTB between 330 to 380 nm, similarly to that previously observed in Eu^{3+}-doped CeO_2 (O→Ce CTB) [34]. The low-relative intensity of CTB in the case of the $La_2Ce_2O_7$ compounds indicates that the probability of the O–Ce charge transfer has been greatly reduced due to a 50% La substituting in the Ce sites. The excitation spectra are dominated by the Eu^{3+} sharp lines at 394, 416, 466 and 535 nm, corresponding to the $^7F_0 \rightarrow {}^5L_6$, $^7F_0 \rightarrow {}^5D_3$, $^7F_0 \rightarrow {}^5D_2$, and $^7F_0 \rightarrow {}^5D_1$ transitions, respectively [35]. It can be noted that the most intense $^7F_0 \rightarrow {}^5D_2$ transition (466 nm) is resonant with the blue emission of commercial InGaN LED chips (Fig. 7a). This means that the Eu^{3+}-doped $La_2Ce_2O_7$ red phosphors may be efficiently excited with a blue-emitting LED light, which has a significant potential in solid-state lighting [36,37]. Fig. 4b shows the emission spectra of $La_2Ce_{2-x}O_{7-x/2}$:xEu (x=0.1–0.9) compound excited at 466 nm. The samples can be effectively excited with 466 nm, and the typical sharp peaks are clearly observed

within the range of 575–725 nm. The strongest emission peaks locate at 615 and 630 nm, which result in the intrinsic red light emission dominated by the Eu^{3+} $^5D_0 \rightarrow {}^7F_2$ transition [38–40].

To demonstrate the ability of the $La_2Ce_2O_7$ compounds as down-shifting phosphors for solid state lighting, the emission features of a selected concentration (x=0.7) were compared to those of the analogous CeO_2 compound ($Ce_{1-y}O_2$:yEu with y=0.18 to keep the same Eu doping content). The emission spectra excited at 466 nm are compared in Fig. 5a. Despite changes in the relative intensity between the Stark components, the spectra reveal the typical intra-$4f^6$ $^5D_0 \rightarrow {}^7F_{0-4}$ transitions. The emission features were quantified by the calculus of the CIE chromaticity coordinates (Fig. 5b) and the absolute emission quantum yield (QY) values, Table 1. Although both phosphors have the same dominant emission, the CIE color coordinates for Eu^{3+}-doped $La_2Ce_2O_7$ and CeO_2 samples are (0.654,0.345) and (0.620,0.379), respectively, and, then, the coordinates of the former phosphor are closer to the standard pure red color value (0.67,0.33). we note that although analogous Eu^{3+}-activated red phosphors involving α-$Eu_2(MoO_4)_3$, $Ba_3Eu(PO_4)_3$, $Ba_3Eu(PO_4)_3$, $CsGd_{0.4}Eu_{0.6}(MnO_4)_2$, $Rb_3EuB_6O_{12}$, and $Eu_2(SO_4)_3$ also display efficient $^5D_0 \rightarrow {}^7F_{0-4}$ transitions, the excitation wavelengths (355 nm, 396 nm and 514.5 nm) do not match the blue emitting LED chip at 466 nm [13,14,38–40].

The QY obtained for $La_2Ce_{2-x}O_{7-x/2}$:xEu (x=0.7), 0.229±0.023, is about 18-fold higher relatively to that of the $Ce_{1-y}O_2$:yEu (y=0.18), 0.013±0.001. Furthermore, to more clearly clarify the luminescence performance of $La_2Ce_{2-x}O_{7-x/2}$:xEu (x=0.7) and $Ce_{1-y}O_2$:yEu (y=0.18), the corrected excitation and emission spectra of the two samples are measured and shown in Fig. S2. Further comparison between the two phosphors was performed by the measurement of the $^5D_0$ emission decay curves (see Fig. S3). These curves are well described by a single-exponential function, and it indicates the presence of a single average Eu^{3+} local coordination site

(replacement of Ce^{4+} in the host), revealing a larger $^5D_0$ lifetime value for $La_2Ce_{2-x}O_{7-x/2}$:xEu(x=0.7) (0.835±0.010 ms) compared to that found for $Ce_{1-y}O_2$:yEu (y=0.18) (0.426±0.010 ms), Table 1.

The distinct $^5D_0$ lifetime values are in good agreement with the variation of the activator Eu^{3+} local coordination in the two lattices. In order to gain deeper insights into such differences, the radiative (k_r) and nonradiative emission decay rates (k_{nr}) were calculated by the Ln luminescence software package (LUMPAC) [41], Table 1. Accordingly, the $^5D_0$quantum efficiency (q) was calculated through [42]:

$$q=k_r/(k_r+k_{nr}) \quad (1)$$

where k_r and k_{nr} denote the radiative and non-radiative probabilities constants, respectively. As shown in Table 1, the enhanced performance of the Eu^{3+}-doped $La_2Ce_2O_7$ compound in reference to that of Eu^{3+}-doped CeO_2 (q values of 0.315 and 0.081, respectively) is due to the higher k_r and lower k_{nr} values. This can be further rationalized via the relative intensity ratio (R) between the $^5D_0\rightarrow{}^7F_2$ and the $^5D_0\rightarrow{}^7F_1$ transitions. It is known that the $^5D_0\rightarrow{}^7F_2$ transition is a forced-electric dipole transition, which is quite sensitive to the local environment around the Eu^{3+} ions. Contrarily, the $^5D_0\rightarrow{}^7F_1$ transition is allowed through the magnetic dipole selection rule and, thus, its intensity is relatively independent of the site symmetry and surroundings of the Eu^{3+} ions [42,43]. Therefore, the intensity ratio R is usually considered as a probe to Eu^{3+} local environment variations in the lattice. In general, the higher the R value, the more Eu^{3+} would occupy sites without an inversion centre [44,45]. The R values for Eu^{3+}-doped $La_2Ce_2O_7$ and CeO_2 are 5.40 and 1.99, respectively (Table 1). Despite the same Eu^{3+} doping content, the two samples show quite different R values (and, then, distinct chromaticity coordinates), which means that the crystal field environment of Eu^{3+} is greatly changed and more Eu^{3+} ions have

294 occupied the asymmetry centre sites in $La_2Ce_2O_7$. The obvious variation of the Eu^{3+}crystal field
295 environment is closely related with the existence of large amounts of oxygen vacancies in the
296 lattice, as shown in the Raman spectra (Fig. 3).

297 Taking advantage of the intriguing emission properties of the Eu^{3+}-doped $La_2Ce_2O_7$, a selected
298 concentration (x=0.7) was used to produce a pure-red emitting device by coating a commercial
299 blue LED chip emitting at 465 nm (Fig. 6). The emitted blue- and downshifted red-light (inset in
300 Fig. 7a) are characterised by pure blue and red color coordinates, (0.131,0.060) and
301 (0.669,0.330), respectively (Fig. 7b). Typically, the performance of an LED is characterized by
302 the wall-plug efficiency (WPE), which accounts for the ratio between the luminous flux (lm) and
303 the electric power (W). A WPE of ~0.4 lm/W was measured in the coated LED demonstrating
304 that the proposed approach has the potential to be applied as a suitable red component in the
305 fabrication of WLEDs.

306 As the Eu^{3+}-doped $La_2Ce_2O_7$pure red emission is attained under analogous conditions found
307 in commercial WLEDs (fabricated combining a blue chip and the YAG:Ce^{3+} commercial yellow
308 phosphor), we can use it to increase the amount of red emission in current WLEDs, which is the
309 principal factor limiting the CCT performance. The WLEDs prototypes (S1 to S5) were
310 fabricated coating a commercial blue chip (465 nm) with blends formed by distinct proportions of
311 YAG:Ce^{3+} and Eu^{3+}-doped La_2Ce_2O (Fig. 7a). As the relative amount of Eu^{3+}-doped La_2Ce_2O
312 increases, the CCT and CRI parameters of the WLEDs are tuned to yield warm white light (Table
313 2).The corresponding chromaticity coordinates are shown in Fig. S4 (ESI†), which results from
314 the balance between the blue emission (~452 nm) ascribed to the blue LED chip, the yellow
315 component (~580 nm) due to YAG:Ce^{3+}phosphor and the red emission peaks (612 and 627 nm)
316 attributed to $^5D_0 \rightarrow {}^7F_2$ transition of Eu^{3+}-doped $La_2Ce_2O_7$ red phosphor. Thus, compared to the

commercial InGaN blue chip and YAG:Ce^{3+} based WLEDs, the blend-based WLEDs have CCT values adjusted from 7119 K (cool white light) to 3242 K (warm white light) and CRI values modulated from 83.9 to 73.0 (Fig. 7b) that are well-above the existing figure of merit.

4. Conclusions

$La_2Ce_{2-x}O_{7-x/2}$:xEu (x=0.1–0.9) red-emitting phosphors have been synthesized by hydrothermal self-rising process using mixed urea/glycine as leavening agents. The phosphors, aspherical/elliptical particles with a diameter about 55±10 nm, are effectively excited at 466 nm presenting for the optimal Eu^{3+}doping concentration (x=0.7) a maximum absolute emission quantum yield of 0.229±0.023. By combining a commercial blue LED chip and the Eu^{3+}-doped $La_2Ce_2O_7$ phosphor, the efficient pure red emission was achieved with color coordinates of (0.669,0.330) and a wall-plug efficiency of ~0.4 lm/W. WLEDs were fabricated combining a blue InGaN LED chip with blends formed by distinct proportions of YAG:Ce^{3+} and Eu^{3+}-doped $La_2Ce_2O_7$. As the relative amount of Eu^{3+}-doped La_2Ce_2O increases, the CCT of the WLEDs is tuned to yield warm white light (from 7119 K, cool white light, to 3242 K, warm white light), whereas the Ra is modulated from 83.9 to 73.0. These results are well-above the existing figure of merit, indicating that these new $La_2Ce_{2-x}O_{7-x/2}$:xEu (x=0.1–0.9) red phosphors are an alternative to Eu^{2+}-based phosphors to enhance the Ra and CCT values of commercial LEDs.

Acknowledgments

The authors would like to thank Dr. Ruilong Zong from Tsinghua University, who helped to measure the Raman spectra of the samples. This work was financially supported by the Natural Science Foundation of Hebei Province (Grant No. E2015205159), the Science Foundation of Hebei Normal University (Grant No. L2019K11) and the China Scholarship Council (Grant No.:

201707920002, 2017–2020), from P.R. China, and CICECO-Aveiro Institute of Materials, FCT (UID/CTM/50011/2019) and WINLEDs (POCI-01-0145-FEDER-030351), from Portugal.

References

[1] A. De Almeida, B. Santos, B. Paolo, M. Quicheron, Solid state lighting review–Potential and challenges in Europe, Renewable Sustainable Energy Rev. 34 (2014) 30–48.

[2] Energy Information Administration, How much electricity is used for lighting in the United States? https://www.eia.gov/tools/faqs/faq.php?id=99&t=3 (accessed 1 July 2019).

[3] E.F. Schubert, J.K. Kim, Solid-state light sources getting smart, Science 308 (2005) 1274–1278.

[4] C.C. Lin, R.S. Liu, Advances in phosphors for light-emitting diodes, J. Phys. Chem. Lett. 2 (2011) 1268–1277.

[5] R. Zhang, H. Lin, Y. Yu, D. Chen, J. Xu, Y. Wang, A new-generation color converter for high-power white LED: transparent Ce^{3+}:YAG phosphor-in-glass, Laser Photonics Rev. 8 (2014) 158–164.

[6] J.J. Li, J.D. Chen, R.F. Wei, H. Guo, Combined white luminescence from Eu^{3+}, ML–Ag particles and Ag^{+} in Ag–Eu^{3+} co□doped H_3BO_3–BaF_2 glasses, J. Am. Ceram. Soc. 95 (2012) 1208–1211.

[7] X. Ma, X. Li, J. Li, C. Genevois, B. Ma, A. Etienne, C. Wan, E. Véron, Z. Peng, M. Allix, Pressureless glass crystallization of transparent yttrium aluminum garnet-based nanoceramics, Nat. Commun. 9 (2018) 1175.

[8] H. Zhu, C.C. Lin, W. Luo, S. Shu, Z. Liu, Y. Liu, J. Kong, E. Ma, Y. Cao, R.S. Liu, and X. Chen, Highly efficient non-rare-earth red emitting phosphor for warm white light-emitting diodes, Nat. Commun. 5 (2014) 4312.

[9] J.H. Li, J. Yan, D.W. Wen, W. U. Khan, J.X. Shi, M.M. Wu, Q. Su and P.A. Tanner, Advanced red phosphors for white light-emitting diodes, J. Mater. Chem. C 4 (2016) 8611–8623.

[10] J.H. Oh, Y.J. Eo, H. C. Yoon, Y.D. Huh, Y.R. Do, Evaluation of new color metrics: guidelines for developing narrow-band red phosphors for WLEDs, J. Mater. Chem. C 4 (2016) 8326–8348.

[11] R.J. Xie, N. Hirosaki, T. Suehiro, F.F. Xu, M. Mitomo, A simple, efficient synthetic route to $Sr_2Si_5N_8$:Eu^{2+}-based red phosphors for white light-emitting diodes, Chem. Mater. 18 (2006) 5578–5583.

[12] Y.Q. Li, G. De With, H.T. Hintzen, Luminescence properties of Ce^{3+}-activated alkaline earth silicon nitride $M_2Si_5N_8$ (M = Ca, Sr, Ba) materials, J. Lumin. 116 (2006) 107–116.

[13] P.L. Shi, Z.G. Xia, M.S. Molokeev, and V.V. Atuchin, Crystal chemistry and luminescence properties of red-emitting $CsGd_{1-x}Eux(MnO_4)_2$ solid-solution phosphors, Dalton Trans. 44 (2014) 9669–9676.

[14] V.V. Atuchin, A.S. Aleksandrovsky, O.D. Chimitova, T.A. Gavrilova, A.S. Krylov, M.S. Molokeev, A.S. Oreshonkov, B.G. Bazarov, and J.G. Bazarova, Synthesis and spectroscopic properties of monoclinic α-$Eu_2(MnO_4)_3$, J. Phys. Chem. C 118 (2014) 15404–15411.

[15] V.V. Atuchin, A.S. Aleksandrovsky, O.D. Chimitova, C.P. Diao, T.A. Gavrilova, V.G. Kesler, M.S. Molokeev, A.S. Krylov, B.G. Bazarov, J.G. Bazarova, Z.S. Lin,

Electronic structure of β-$RbSm(MoO_4)_2$ and chemical bonding in molybdates, Dalton Trans. 44 (2015) 1805–1815.

[16] P.F. Smet, A.B. Parmentier, D. Poelman, Selecting Conversion Phosphors for White Light-Emitting Diodes, J. Electrochem. Soc. 158 (2011) R37–R54.

[17] E. Song, J. Wang, J. Shi, T. Deng, S. Ye, M. Peng, J. Wang, L. Wondraczek, Q. Zhang, Highly efficient and thermally stable $K_3AlF_6:Mn^{4+}$ as a red phosphor for ultra-high-performance warm white light-emitting diodes, ACS Appl. Mater. Interfaces 9 (2017) 8805 8812.

[18] L. Huang, Y. Liu, J. Yu, Y. Zhu, F. Pan, T. Xuan, M.G. Brik, C. Wang, Highly stable $K_2SiF_6:Mn^{4+}@K_2SiF_6$ composite phosphor with narrow red emission for white LEDs, J. Wang, ACS Appl. Mater. Interfaces 10 (2018) 18082–18092.

[19] G. Vimal, K. P. Mani, P. R. Biju, C. Joseph, N.V. Unnikrishnan, M.A. Ittyachen, Structural studies and luminescence properties of $CeO_2:Eu^{3+}$ nanophosphors synthesized by oxalate precursor method, Appl. Nanosci. 5 (2015) 837–846.

[20] J. Meyer, F. Tappe, Photoluminescent materials for solid□State lighting: State of the art and future challenges, Adv. Opt. Mater. 3 (2015) 424.

[21] S.K. Shi, K.Y. Li, S.P. Wang, R.L. Zong, G.L. Zhang, Structural characterization and enhanced luminescence of Eu-doped $2CeO_2–0.5La_2O_3$ composite phosphor powders by a facile solution combustion synthesis, J. Mater. Chem. C 5 (2017) 4302–4309.

[22] H.S. Zhang, X.G. Chen, G. Li, X.L. Wang, X.D. Dang, Influence of Gd2O3 addition on thermophysical properties of La2Ce2O7 ceramics for thermal barrier coatings, J. Eur. Ceram. Soc. 32 (2012) 3693–3700.

[23] Q.P. Zhang, X. Zheng, J. Jiang, W. Liu, Structural Stability of $La_2Ce_2O_7$ as a Proton Conductor: A First-Principles Study, J. Phys. Chem. C 117 (2013) 20379–20386.

410 [24] S. Shi, Y. Yang, P. Guo, J. Wang, L. Geng, L.S. Fu, Improved morphology and
411 optimized luminescence of Eu^{3+}-doped $La_2Ce_2O_7$ composite nanopowders by
412 surfactant-assisted solution combustion synthesis, J. Lumin. 206 (2019) 91–96.
413 [25] M. Wolcyrz, L. Kepinski, Rietveld refinement of the structure of CeOCI formed in
414 Pd/CeO_2 catalyst: Notes on the existence of a stabilized tetragonal phase of La_2O_3 in
415 La–Pd–O system, J. Solid State Chem. 99 (1992) 409–413.
416 [26] H.K. Müller-Buschbaum, H.G.V. Schnering, Zur struktur der a-form der sesquioxide
417 der seltenen erden. strukturuntersuchungen an La_2O_3, Z. Anorg. Allg. Chem. 340 (1956)
418 232–245.
419 [27] M.S. Bakshi, How surfactants control crystal growth of nanomaterials, Cryst. Growth
420 Des. 16 (2016) 1104–1133.
421 [28] Y. Wang, C. Wang, C. Li, Y. Cheng, F. Chi, Influence of different surfactants on
422 crystal growth behavior and sinterability of $La_2Ce_2O_7$ solid solution, Ceram. Int. 40
423 (2014) 4305–4310.
424 [29] J.J. Wu, S.K. Shi, X.L. Wang, H.H. Song, M. Luo, W. Chen, Self-rising synthesis and
425 luminescent properties of Eu^{3+}-doped nanoceria, J. Lumin. 152 (2014) 142–144.
426 [30] N.O. Nuñez, S.R. Liviano, M. Ocaña, Citrate mediated synthesis of uniform monazite
427 $LnPO_4$ (Ln= La, Ce) and Ln: $LaPO_4$ (Ln= Eu, Ce, Ce+Tb) spheres and their
428 photoluminescence, J. Colloid Interface Sci. 349 (2010) 484–491.
429 [31] V.G. Keramidas, W.B. White, Raman spectra of oxides with the fluorite structure, J.
430 Chem. Phys. 59 (1973) 1561–1562.
431 [32] Z.D. Dohčević-Mitrović, M.J. Šćepanović, M.U. GrujićBrojčin, Z.V. Popović, S.B.
432 Bošković, B.M. Matović, M.V. Zinkevich, F. Aldinger, The size and strain effects on

433 the Raman spectra of $Ce_{1-x}Nd_xO_{2-\delta}$ ($0 \leq x \leq 0.25$) nanopowders Solid State Commun.
434 137 (2006) 387–390.
435 [33] D. Avram, M. Sanchez-Dominguez, B. Cojocaru, M. Florea, V. Parvulescu, C. Tiseanu,
436 Toward a unified description of luminescence–local structure correlation in Ln doped
437 CeO_2 nanoparticles: Roles of Ln ionic radius, Ln concentration, and oxygen vacancies,
438 J. Phys. Chem. C 119 (2015) 16303–16313.
439 [34] S.K. Shi, M. Hossu, R. Hall, W. Chen, Solution combustion synthesis,
440 photoluminescence and X-ray luminescence of Eu-doped nanoceria CeO_2:Eu, J. Mater.
441 Chem. 22 (2012) 23461–23467.
442 [35] K. Binnemans, Interpretation of europium(III) spectra, Coord. Chem. Rev. 295 (2015)
443 1–45.
444 [36] X. Huang, Solid-state lighting: Red phosphor converts white LEDs, Nat. Photonics 8
445 (2014) 748–749.
446 [37] Z. Xia, Q. Liu, Progress in discovery and structural design of color conversion
447 phosphors for LEDs, Prog. Mater. Sci. 84 (2016) 59–117.
448 [38] H.P. Ji, Z.H. Huang, Z.G. Xia, M.S. Molokeev, X.X Jiang, Z.S. Lin, V.V. Atucin,
449 Comparative investigations of crystal structure and photoluminescence property of
450 eulytite-type $Ba_3Eu(PO_4)_3$ and $Sr_3Eu(PO_4)_3$, Dalton Trans. 44 (2015) 7679–7686.
451 [39] V.V. Atuchin, A.K. Subanakov, A.S. Aleksandrovsky, B.G. Bazarov, J.G. Bazarova,
452 T.A. Gavrilova, A.S. Krylov, M.S. Molokeev, A.S. Oreshonkov, S.Y. Stefanovich,
453 Structural and spectroscopic properties of new noncentrosymmetric self-activated
454 borate $Rb_3EuB_6O_{12}$ with B_5O_{10} units, Mater. Des. 140 (2018) 488–494.
455 [40] Y.G. Denisenko, A.S. Aleksandrovsky, V.V. Atuchin, A.S. Krylov, M.S. Molokeev,
456 A.S. Oreshonkov, N.P. Shestakov, O.V. Andreev, Exploration of structural, thermal

457 and spectroscopic properties of self-activated sulfate $Eu_2(SO_4)_3$ with isolated SO_4
458 groups, J. Indust. Eng. Chem. 68 (2018) 109–116.
459 [41] J.D.L. Dutra, T.D. Bispo, R.O. Freire, LUMPAC lanthanide luminescence software:
460 efficient and user friendly, J. Comput. Chem. 35 (2014) 772–775.
461 [42] L.D. Carlos, R.A.S. Ferreira, V. de Zea Bermudez, and S.J.L. Ribeiro,
462 Lanthanide□containing light□emitting organic–inorganic hybrids: A bet on the future,
463 Adv. Mater. 21 (2009) 509–534.
464 [43] P.A. Tanner, Some misconceptions concerning the electronic spectra of tri-positive
465 europium and cerium, Chem. Soc. Rev. 42 (2013) 5090–5101.
466 [44] G. Blasse, B. C. Grabmaier, Luminescent Materials, first ed., Springer-Verlag, Berlin,
467 1994.
468 [45] H. Li, R. Zhao, Y. Jia, W. Sun, J. Fu, L. Jiang, S. Zhang, R. Pang, C. Li, $Sr_{1.7}Zn_{0.3}CeO_4$:
469 Eu^{3+}, novel red-emitting phosphors: synthesis and photoluminescence properties, ACS
470 Appl. Mater. Interfaces 6 (2014) 3163–3169.
471
472
473
474
475
476
477
478
479
480

Figure captions

Fig. 1. XRD patterns of the a) samples prepared with single urea (black color pattern), mixed urea/glycine as leavening agent (red color), as well as the standard references of CeO_2 and La_2O_3; b) $La_2Ce_{2-x}O_{7-x/2}$:xEu^{3+} (x=0–0.9) composite powders prepared by a hydrothermal self-rising reaction (with mixed urea/glycine as leavening agent) and a subsequent sintering process.

Fig. 2. SEM images of the a) Eu^{3+}-doped $La_2Ce_2O_7$ precursor and b) composite powders after a sintering process. c) Particle size distribution in b).

Fig. 3. FT-Raman spectra of $La_2Ce_{2-x}O_{7-x/2}$:xEu(x=0.1, 0.7).

Fig. 4. Room-temperature a) excitation spectra monitored at 615 nm and b) emission spectra excited at 466 nm of $La_2Ce_{2-x}O_{7-x/2}$:xEu(x=0.1–0.9).

Fig. 5. a) Emission spectra of $La_2Ce_{2-x}O_{7-x/2}$:xEu (x=0.7) and $Ce_{1-y}O_2$:yEu (y=0.18) excited at 466 nm and b) CIE chromaticity diagram (1931) showing the (x,y) emission chromaticity coordinates.

Fig. 6. a) Emission spectra, and photographs, of the commercial LED and of the Eu^{3+}-doped $La_2Ce_2O_7$ red-emitting LEDs operating under forward-bias current of 20×10^{-3} A; b) CIE chromaticity diagram (1931) showing the (x,y) emission chromaticity coordinates of original and coated LEDs.

Fig. 7. Room temperature a) emission spectra of S1 to S5 WLEDs. The inset shows photographs of the devices. b) Relationship between CCT and CRI and the amount of blend phosphors used (the lines are visual guides).

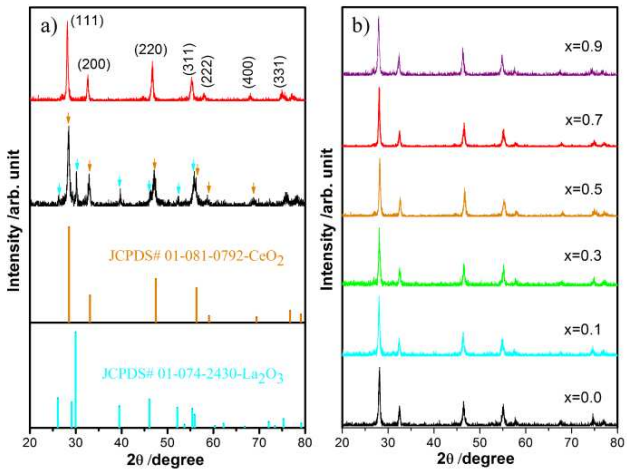

503

504 **Fig. 1**

505

506

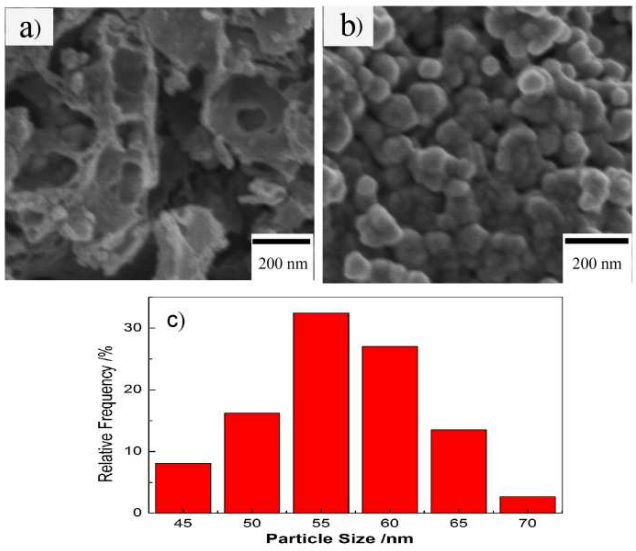

507

508 **Fig. 2**

509

510

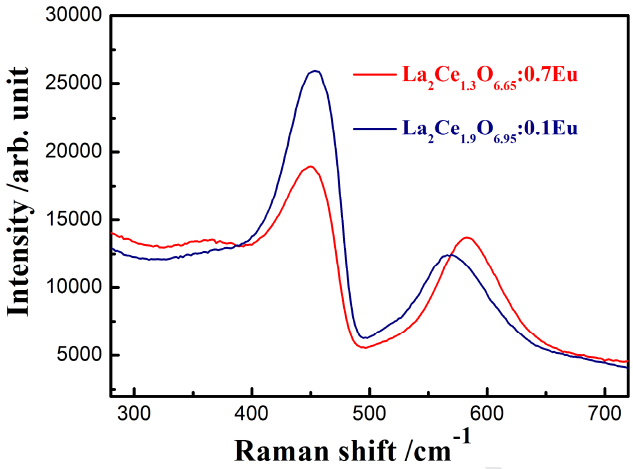
30000
25000
20000
15000
10000
5000
Intensity /arb. unit
300
400
500
600
700
Raman shift /cm-1
La2Ce1.3O6.65:0.7Eu
La2Ce1.9O6.95:0.1Eu

Fig. 3

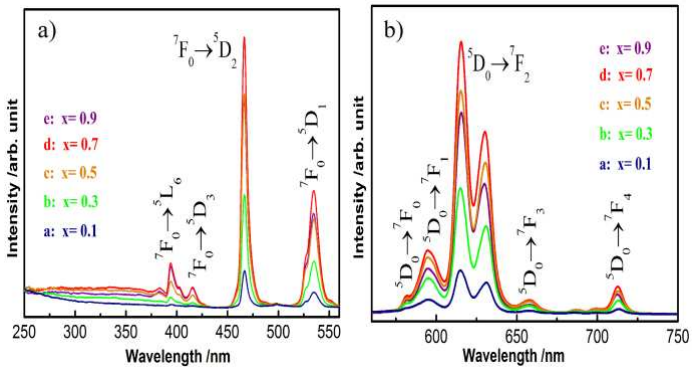
a)
7F0→5D2
7F0→5L6
7F0→5D3
7F0→5D1
e: x= 0.9
d: x= 0.7
c: x= 0.5
b: x= 0.3
a: x= 0.1
Intensity /arb. unit
250
300
350
400
450
500
550
Wavelength /nm
b)
5D0→7F2
5D0→7F0
5D0→7F1
5D0→7F3
5D0→7F4
e: x= 0.9
d: x= 0.7
c: x= 0.5
b: x= 0.3
a: x= 0.1
Intensity /arb. unit
600
650
700
750
Wavelength /nm

Fig. 4

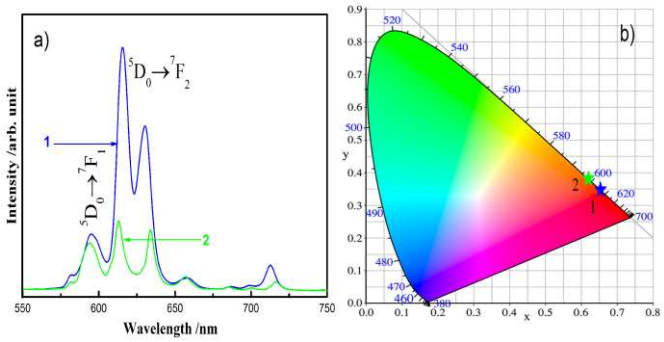
a)
$^5D_0 \rightarrow {}^7F_2$
$^5D_0 \rightarrow {}^7F_1$
1
2
Intensity /arb. unit
Wavelength /nm
b)
x
y
1
2

Fig. 5

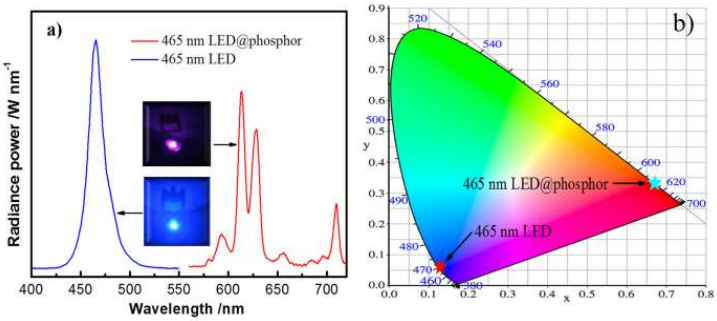
a)
465 nm LED@phosphor
465 nm LED
Radiance power /W nm^{-1}
Wavelength /nm
b)
x
y
465 nm LED@phosphor
465 nm LED

Fig. 6

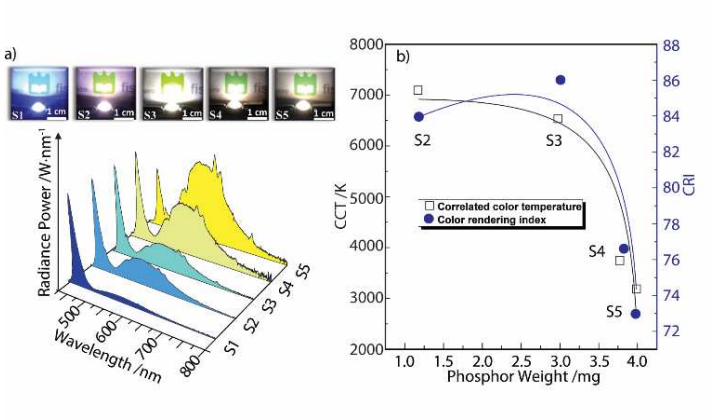

Fig. 7

565 **Table legends**

566 **Table 1** Photophysical data of $La_2Ce_{2-x}O_{7-x/2}$:xEu (x=0.7) and $Ce_{1-y}O_2$:yEu (y=0.18).

567 **Table 2** Optical parameters of WLEDs (S1 to S5) and blue chip (S0).
568

569

570 **Table 1**

Composite	τ (ms)	k_r (s^{-1})	k_{nr} (s^{-1})	R	q	QY
$La_2Ce_2O_7$:Eu	0.835±0.010	377.0	820.7	5.40	0.315	0.229±0.023
CeO_2:Eu	0.427±0.010	190.2	2157.2	1.99	0.081	0.013±0.001

571

572 **Table 2**

LEDs	Luminous flux (mlm)	LE (lm/W)	Color coordinates (x, y)	CRI	CCT (K)	Coating phosphor (mg)
S0	405.36	31.18	(0.131, 0.060)			0
S1	346.65	22.22	(0.204, 0.118)			0.7
S2	235.04	18.08	(0.311, 0.289)	83.9	7119	1.2
S3	125.67	9.67	(0.318, 0.289)	86.0	6533	3.0
S4	69.47	5.34	(0.381, 0.352)	76.7	3778	3.8
S5	61.79	4.75	(0.432, 0.425)	73.0	3242	4.0

573

574

575 **TOC**

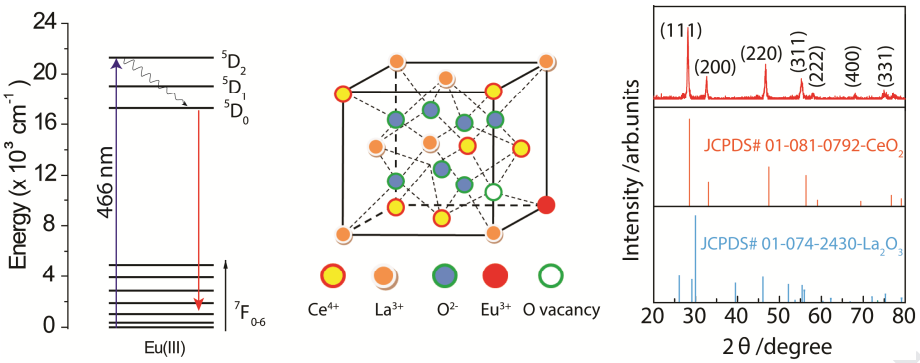

576

Highlights

- Eu^{3+}-activated $La_2Ce_2O_7$ phosphors can be efficiently excited by blue light LED
- Phosphors can emit strong red colour with quantum yield of 0.229
- WLEDs were fabricated by coating blue LED with YAG:Ce^{3+} and Eu^{3+}-activated $La_2Ce_2O_7$
- Colour rendering index and correlated colour temperature can be easily adjusted